CLM-P838

A non-linear model of the sawtooth collapse in tokamaks

C. M. Bishop
S. C. Cowley

UK ATOMIC ENERGY AUTHORITY

Culham Laboratory

CLM-P838

A non-linear model of the sawtooth collapse in tokamaks

C.M. Bishop, S.C. Cowley[‡]

Culham Laboratory, Abingdon, Oxon. OX14 3DB, England

(Euratom/UKAEA Fusion Association)

[‡]Princeton Plasma Physics Laboratory, Princeton, N.J., U.S.A.

Abstract

The usual resistive reconnection models of the sawtooth phenomenon in tokamaks are inconsistent with recent experimental data from the large devices such as JET. A more likely description involves an ideal motion during the collapse phase, associated with an almost flat q-profile. In this paper we present a non-linear calculation of the final plasma configuration resulting from any initial equilibrium having $q = 1$ over some central region. The problem is formulated both in cylindrical and toroidal geometry, and solved for example profiles.

(Submitted to Physics of Fluids)

March 1988

I. Introduction.

One of the remarkable features of the sawtooth phenomenon in the larger tokamaks such as JET is the fast timescale of the collapse [1], which appears to be inconsistent with the original picture of the sawtooth proposed by Kadomstev [2]. This assumed a q-profile which increased monotonically towards the outside of the plasma and which had a single $q = 1$ surface. The collapse phase corresponded to an $m = 1$, $n = 1$ mode leading to resistive reconnection within the $q = 1$ surface and a flattening of the q-profile in the inner region of the plasma. The original q-profile was then restored by resistive diffusion of the current profile during the ramp phase.

In JET, however, resistive diffusion during the ramp is so slow [3] that q can only change by an amount $\delta q/q \sim 10^{-2}$, so that a q-profile once flattened, will remain essentially flat. Furthermore, for the monotonic q-profile of Kadomstev the linear eigenfunction is a rigid displacement of the plasma core:

$$\xi_R = \xi_0 \qquad r < r(q=1)$$

$$\xi_R = 0 \qquad r > r(q=1) \tag{1}$$

Soft X-ray tomography on JET [4] (which measures $\sim n^2T^2 \sim p^2$) shows that the plasma motion during the collapse is quite different from this. Fig. 1a shows the plasma profile immediately before the collapse. The

initial phase of the collapse is shown in Fig. 1b and represents an interchange of the hot core and the colder plasma surrounding it. The final state at the end of the collapse, shown in Fig. 1c, is again axisymmetric. Note that the pressure profile is now hollow. Finally, the timescale of the collapse (~100 μs in JET) is too fast for significant resistive reconnection to take place. This suggests that an ideal MHD motion is involved.

Wesson [3] has suggested that the q-profile in JET is essentially flat and equal to unity up to some radius, and then increases monotonically. An example of such a profile is shown in Fig. 2. The corresponding ideal internal kink mode gives a convective flow pattern [3,5] which corresponds well to the soft X-ray tomography results.

In this paper we shall present a non-linear model of the sawtooth collapse based on the type of q-profile shown in Fig. 2. When q is exactly equal to unity in the inner region, the field lines join onto themselves after a single transit of the torus. There is no shear in the magnetic field, and ideal MHD permits the free interchange of flux tubes. This allows the final configuration of the plasma at the end of the crash phase to be calculated for a given initial equilibrium. The calculation makes no linearity approximation and does not require knowledge of the detailed route by which the final state is reached. Any final state which is accessible by ideal MHD is automatically considered. In section II we present the calculation in cylindrical geometry; this allows the physics to be discussed in a situation which is algebraically simple. A general formulation in toroidal geometry is given in section III, and the

equations are solved for an example equilibrium in section IV using the large aspect ratio expansion. The importance of the results is discussed in section V. Appendix A describes a procedure for solving the equations at finite aspect ratio; and a calculation including the effects of the plasma outside the q = 1 surface is given in appendix B.

II. Interchange of Flux Tubes in Cylindrical Geometry.

Consider a tokamak having the q-profile shown in Fig. 2. Within the surface $r = a$ each field line is a closed loop, topologically linked with every other. However, ideal MHD permits the free interchange of these field lines. For a given initial equilibrium we can consider those states which are accessible by such interchanges. The particular route by which the final state is reached is unimportant and only the mapping of initial field lines into final field lines need be considered. No linearity approximation is made, and indeed the final state may be very far removed from the initial one. Since we wish to calculate the configuration at the end of the sawtooth collapse we shall consider only axi-symmetric final states. In the case of cylindrical geometry this allows us to consider the mapping of field lines at radius r_0 in the initial equilibrium into field lines at r in the final state, with a mapping function defined by

$$r = F(r_0) \tag{2}$$

Clearly the mapping should be (locally) continuous, and 1 to 1. This requires that the function F be monotonic. We shall begin by confining our attention to the region $0 \leq r \leq a$ and suppose that there is a rigid wall at $r = a$. The modifications due to the plasma outside $r = a$ are described in appendix B.

The initial plasma state satisfies the cylindrical equilibrium

equation

$$\frac{dp_0}{dr_0} + \frac{1}{2}\frac{dB_{\theta 0}^2}{dr_0} + \frac{1}{2}\frac{dB_{Z0}^2}{dr_0} + \frac{B_{\theta 0}^2}{r_0} = 0 \qquad (3)$$

where p_0 is the initial pressure profile, and $B_{\theta 0}$, B_{Z0} are the initial magnetic field components. Since $q = 1$ throughout the region considered we have

$$q \equiv \frac{r_0 B_{Z0}}{\bar{R}\, B_{\theta 0}} = 1 \qquad (4)$$

where $\bar{R}$ plays the rôle of the tokamak major radius.

The plasma in the annulus $r_0 \to r_0 + dr_0$ will move to a corresponding annulus $r \to r + dr$ in the final state where $dr = F'(r_0)dr_0$. This motion is subject to two constraints:

(1) conservation of flux. This follows from ideal MHD and for the Z-component of magnetic field it implies

$$B_Z r\,|dr| = B_{Z0} r_0\,|dr_0| \qquad (5)$$

i.e.

$$B_Z(r) = B_{Z0}(r_0)\left|\frac{r_0}{F'F}\right| \qquad (6)$$

where primes denote differentiation with respect to r_0.

A similar relation holds for B_θ, but we can instead simply use the fact that $q = 1$ is preserved by the ideal MHD motions, so that in the final configuration

$$B_\theta = \frac{rB_Z}{\bar{R}} \, . \tag{7}$$

(2) conservation of entropy. The MHD timescale is very short compared to the characteristic thermal conduction time. The motion is essentially adiabatic and we have

$$p(r)^{1/\gamma} \, r|dr| = p_0(r_0)^{1/\gamma} r_0 |dr_0| \tag{8}$$

i.e.

$$p(r) = p_0(r_0) \left| \frac{r_0}{F'F} \right|^\gamma \tag{9}$$

The final axisymmetric configuration is stationary on the MHD timescale and thus satisfies radial force balance. We can therefore write a final state equilibrium equation

$$\frac{dp}{dr} + \frac{1}{2} \left(1 + \frac{r^2}{\bar{R}^2}\right) \frac{dB_Z^2}{dr} + \frac{2r}{\bar{R}^2} B_Z^2 = 0 \tag{10}$$

where we have made use of eq.(7) to eliminate B_θ.

We now express the final state quantities in eq.(10) in terms of initial state quantities, using eqs. (2), (6) and (9), to give

$$\frac{1}{F'}\frac{d}{dr_0}\left\{p_0(r_0)\left|\frac{r_0}{F'F}\right|^\gamma\right\}+\frac{1}{2}\frac{1}{F'}\left(1+\frac{F^2}{\bar{R}^2}\right)\frac{d}{dr_0}\left\{B_{Z0}^2\left|\frac{r_0}{F'F}\right|^2\right\}$$

$$+\frac{2F}{\bar{R}^2}B_{Z0}^2\left|\frac{r_0}{F'F}\right|^2=0 \qquad (11)$$

It is convenient to introduce the notation:

$$x=\frac{r_0^2}{\bar{R}^2}\ ,\quad h=1+\frac{F^2}{\bar{R}^2}\ ; \qquad (12)$$

then eq.(11) becomes

$$\frac{d}{dx}\left\{p_0\left|\frac{dh}{dx}\right|^{-\gamma}\right\}+\frac{1}{2}h\frac{d}{dx}\left\{B_{Z0}^2\left|\frac{dh}{dx}\right|^{-2}\right\}+B_Z^2\left(\frac{dh}{dx}\right)^{-1}=0 \qquad (13)$$

This is a non-linear equation which determines the mapping function $h(x)$ once the initial equilibrium has been specified. Note that the identity map $h(x) = 1 + x$ is clearly a solution.

We can also give a variational formulation in terms of the final state energy functional

$$W_f = 4\pi^2\bar{R} \int_0^a r\, dr \left\{ \frac{p(r)}{\gamma - 1} + \frac{B_\theta^2}{2} + \frac{B_Z^2}{2} \right\} . \qquad (14)$$

Expressing this in terms of initial state quantities, and the mapping function $h(x)$, we obtain

$$W_f[h] = 2\pi^2\bar{R}^3 \int_0^e dx \left\{ \frac{p_0}{\gamma-1} \left| \frac{dh}{dx} \right|^{1-\gamma} + \frac{B_{Z0}^2}{2} h \left| \frac{dh}{dx} \right|^{-1} \right\} \qquad (15)$$

where $e = a^2/\bar{R}^2$. Requiring $W_f[h]$ to be stationary with respect to variations in $h(x)$ then gives eq.(13).

We end this discussion of cylindrical geometry by finding the mapping $h(x)$ for an example equilibrium given by

$$p_0(x) = b_0^2 (\beta e - x) , \qquad B_{Z0}^2 = b_0^2 \qquad (16)$$

where b_0 and β are constants. Clearly eq.(16) is a solution of eq.(3), with $q = 1$. We now seek a solution of eq. (13) corresponding to an inverse monotonic map, i.e., one satisfying the boundary conditions

$$F(r_0 = 0) = a, \qquad F(r_0 = a) = 0 . \qquad (17)$$

We write the mapping in the form

$$h(x) = 1 + e - x + Y(x) \tag{18}$$

where $Y = 0(e^2)$. Substituting into eq. (13), expanding in $e<<1$, and making use of eq.(3), we obtain

$$Y(x) = -x(e - x) \tag{19}$$

This mapping is plotted in Fig. 3 for $e = 0.1$. We can check that the final state has lower energy than the initial state by evaluating eq.(15) both for this map, and for the identity map $h(x) = 1 + x$. These give

$$\frac{W_i}{\pi^2 \bar{R}^3 b_0^2} = e + (3\beta - 1)e^2$$

$$\frac{W_f}{\pi^2 \bar{R}^3 b_0^2} = e + (3\beta - 1)e^2 - \frac{1}{3} e^3 + 0(e^4)$$

for the initial and final energies respectively. The final pressure profile is easily found from eq.(9), and is plotted in Fig.4, again for $e = 0.1$. We see that the initial equilibrium can relax to a state of lower energy, having a hollow pressure profile. This result is in accord with the JET results shown in Fig.1.

The reduction in the plasma potential energy at $O(e^3)$ leads to an increase in kinetic energy which will be dissipated, through viscosity, as heat. This will result in a correction to the pressure profile plotted in Fig.4 of $O(e)$ which can be neglected.

III. Toroidal Geometry.

We now formulate the interchange calculation in general axisymmetric toroidal geometry. Consider a fluid element of volume dV_0 at position $\underline{X}_0$ undergoing a finite displacement to position $\underline{X}$ ($\underline{X}_0$) with final volume dV. We define the Jacobian J by

$$dV = J dV_0 \tag{20}$$

Now imagine the displacement of a small flux tube of length $d\underline{r}_0$, cross-sectional area (normal to the field) dA_0 and field strength $\underline{B}_0$. Using the flux-freezing property of ideal MHD, the final field strength will be

$$| \underline{B} | = | \underline{B}_0 | \, dA_0 / dA \tag{21}$$

where dA is the final cross sectional area. From the chain rule we then have

$$\underline{B} = \frac{| \underline{B} |}{| d\underline{r} |} d\underline{r} = \frac{| \underline{B}_0 | dA_0}{| d\underline{r} | dA} d\underline{r}_0 \cdot (\nabla_0 \underline{r})$$

$$= \frac{1}{J} \underline{B}_0 \cdot \nabla_0 \underline{r} \tag{22}$$

where ∇_0 denotes the gradient operator with respect to the initial coordinate $\underline{r}_0$, and we have made use of eq.(20). Again we consider the

mapping of an initial equilibrium with pressure p_0 into a final equilibrium with pressure p. From entropy conservation we have

$$p = p_0 J^{-\gamma}. \tag{23}$$

The initial and final equilibria satisfy

$$\underline{B}_0 \cdot \nabla_0 p_0 = 0 \tag{24}$$

$$\underline{B} \cdot \nabla p = 0 \quad . \tag{25}$$

Using eq.(22) we then have

$$\underline{B} \cdot \nabla (p_0 J^{-\gamma}) = \frac{1}{J} \underline{B}_0 \cdot (\nabla_0 \underline{r}) \cdot \nabla (p_0 J^{-\gamma})$$

$$= -\gamma p_0 J^{-\gamma-2} \underline{B}_0 \cdot \nabla_0 J = 0$$

and therefore

$$\underline{B}_0 \cdot \nabla_0 \cdot J = 0$$

Thus the Jacobian J is constant along an initial field line. However, these lines lie on constant p_0 surfaces, and hence by axisymmetry

$$J = J(p_0). \tag{26}$$

Eq.(26) implies that initial pressure surfaces are mapped into final pressure surfaces (as was the case in the cylinder). This result considerably simplifies the toroidal formulation.

To proceed further it is convenient to introduce a straight field line coordinate system (r_0, θ_0, ϕ) to describe the initial equilibrium, where ϕ is the usual toroidal angle, and

$$\nabla_0 r_0 \cdot (\nabla_0 \theta_0 \times \nabla_0 \phi) = \frac{\bar{R}}{r_0 R_0^2} \tag{27}$$

where $\bar{R}$ is constant, and $R_0 = R_0(r_0, \theta_0)$ is the major radius. The magnetic field in these coordinates is given by [6]:

$$\underline{B}_0 = \bar{B}\,\bar{R}\,\{f_0(r_0)\,\nabla_0 r_0 \times \nabla_0 \phi + g_0(r_0)\,\nabla_0 \phi\} \tag{28}$$

From eq.(24) it follows that $p_0 = p_0(r_0)$, so that r_0 is a pressure surface label. The safety factor is given by

$$q_0(r_0) \equiv \frac{\underline{B}_0 \cdot \nabla_0 \phi}{\underline{B}_0 \cdot \nabla_0 \theta_0} = \frac{r_0 g_0}{\bar{R} f_0} . \tag{29}$$

We can write an analogous coordinate system for the final state (with the same notation but omitting the suffix), in which r is a final pressure surface label, and hence $r = r(r_0)$, $\theta = \theta(r_0, \theta_0)$. Using eq.(27) the

Jacobian J can then be written

$$J = \frac{R^2}{R_0^2} \frac{dr^2}{dr_0^2} \frac{\partial\theta}{\partial\theta_0} . \tag{30}$$

If we integrate eq.(30) over θ_0 and demand periodicity, we obtain

$$J = \frac{dr^2}{dr_0^2} \frac{1}{< R_0^2/R^2 >} \tag{31}$$

where the flux surface average is defined by

$$< Q > \equiv \frac{1}{2\pi} \int_0^{2\pi} Q \, d\theta \tag{32}$$

From eqs.(30) and (31) we then have

$$\frac{\partial\theta}{\partial\theta_0} = \frac{R_0^2}{R^2} \frac{1}{<R_0^2/R^2>} \tag{33}$$

Finally the conservation of flux in ideal MHD allows us to relate $f(r)$ and $g(r)$ to the corresponding initial quantities $f_0(r_0)$ and $g_0(r_0)$. Consider an axisymmetric ribbon of area ΔA_0 joining two pressure surfaces r_0 and $r_0 + \Delta r_0$ in the initial equilibrium. The poloidal field which intersects this ribbon is given by

$$\bar{B}\ \bar{R}\ f_0(r_0)\ \frac{|\nabla_0 r_0|}{R_0} \tag{34}$$

while the area of the ribbon is

$$2\pi R_0\ \frac{\Delta r_0}{|\nabla_0 r_0|} \tag{35}$$

and hence the flux which intersects this ribbon is

$$2\pi \bar{B}\ \bar{R}\ f_0(r_0)\ \Delta r_0. \tag{36}$$

This must equal the flux which intersects the corresponding ribbon in the final equilibrium, given by

$$2\pi \bar{B}\ \bar{R}\ f(r)\ \Delta r \tag{37}$$

and hence f(r) is given by

$$f(r) = f_0(r_0)\left|\ \frac{dr_0}{dr}\ \right|. \tag{38}$$

The safety factor in the final equilibrium will be

$$q(r) = \frac{r\ g(r)}{\bar{R}\ f(r)} \tag{39}$$

which together with eq. (29) and (38) gives the equation for $g(r)$:

$$g(r) = g_0(r_0)\left|\frac{dr_0^2}{dr^2}\right| . \tag{40}$$

Eqs. (23), (31), (33), (38) and (40), together with the initial and final equilibrium (Grad-Shafanov) equations constitute a complete set of equations determining the allowed final states for any given initial equilibrium. In the next section we shall find a solution for an example equilibrium using the large aspect ratio expansion.

IV. Large Aspect Ratio Solution.

Using the standard tokamak ordering $p/B^2 \sim \varepsilon^2$, $f \sim \varepsilon$, $g \sim 1$, (where ε is the inverse aspect ratio) we can find solutions of the Grad-Shafanov equation in terms of the straight field line coordinates introduced in the previous section. These solutions have the form of nested circles (to lowest order) with major radius coordinate $R(r, \theta)$ given by [6]:

$$R^2 = \bar{R}^2\{1 - \frac{2r}{\bar{R}} \cos\theta - \frac{2\Delta}{\bar{R}} - \frac{r}{\bar{R}} \frac{d\Delta}{dr} - \frac{1}{2} \frac{r^2}{\bar{R}^2} \} \tag{41}$$

where harmonic terms have been omitted at highest order (we shall see that they do not contribute to the energy functional), and where $\Delta(r)$ represents the shift of the centres of the flux surfaces. Expanding the Grad-Shafanov equation we find that $g = 1 + \varepsilon^2 g^{(2)}$, and

$$\frac{p}{\bar{B}^2} + g_2' + \frac{f}{r}(rf)' = 0 \tag{42}$$

$$\Delta'' + \{\frac{2}{rf}(rf)' - \frac{1}{r}\}\Delta' - \frac{1}{\bar{R}} + \frac{2r}{\bar{R}f^2} \frac{p'}{\bar{B}^2} = 0 \tag{43}$$

where primes denote differentiation with respect to r. Anologous equations hold for the initial equilibrium. As for the cylinder we can find the mapping function, which we write in the form:

$$r^2 = a^2 - r_0^2 + Y(r_0^2) \tag{44}$$

where a is the boundary of the $q = 1$ region, and is taken to be fixed. Using eq.(40) we have

$$g^{(2)}(r) = g_0^{(2)}(r_0) + \frac{dY}{dr_0^2} . \tag{45}$$

The initial and final equilibrium equations, together with $q = 1$, then give

$$Y(r_0^2) = -r_0^2 (a^2 - r_0^2) / \bar{R}^2 . \tag{46}$$

If we define $x = r_0^2/\bar{R}^2$, and $e = a^2/\bar{R}^2$ we have

$$\frac{r^2}{\bar{R}^2} = e - x - x(e - x). \tag{47}$$

Note that to this order the mapping is independent of the particular initial equilibrium.

The final state energy is given by

$$W_f = \int \left(\frac{p}{\gamma-1} + \frac{B^2}{2}\right) dV \tag{48}$$

with volume element

$$dV = JdV_0 = \left| \frac{dr^2}{dr_0^2} \right| \frac{1}{\langle R_0^2/R^2 \rangle} \frac{R^2_0 r_0}{\bar{R}} dr_0 d\theta_0 . \tag{49}$$

Performing the θ_0 integration then gives

$$\frac{W_f}{\pi^2 \bar{R}^3 \bar{B}^2} = \frac{1}{2} \int_0^1 g_0^2 \left| \frac{dr_0^2}{dr^2} \right| dx$$

$$+ \frac{1}{2} \int_0^1 f_0^2 \left| \frac{dr_0^2}{dr^2} \right| \left\langle \frac{|\nabla r|^2 R_0^2}{R^2} \right\rangle \left| \frac{dr^2}{dr_0^2} \right| \frac{1}{\langle R_0^2/R^2 \rangle} dx$$

$$+ \frac{3}{2} \int \frac{p_0}{\bar{B}^2} \left[\left| \frac{dr^2}{dr_0^2} \right| \frac{1}{\langle R_0^2/R^2 \rangle} \right]^{-2/3} \frac{\langle R_0^2 \rangle}{\bar{R}^2} dx \tag{50}$$

where we have taken $\gamma = 5/3$.

It is convenient at this point to introduce a specific example for the initial equilibrium. Following the cylindrical calculation we choose $g_0(r_0) = 1$ to all orders, giving (for $q = 1$), $f_0^2 = x$, and

$$\frac{p_0}{\bar{B}^2} = \beta e - x \tag{51}$$

where β is a constant of order unity.

To evaluate the various terms in W_f to the order required, we need

the $0(\varepsilon)$ terms in $\theta(\theta_0, r_0)$. These are obtained by integrating eq.(33) to give :

$$\cos\theta = \cos\theta_0 - \frac{(r - r_0)}{\bar{R}} \tag{52}$$

where again harmonic terms at highest order have been discarded.

Next we need to find expressions for $\Delta(r)$ and $\Delta_0(r_0)$. From eq.(43) , together with $q = 1$, we have

$$\frac{d}{dr^2}\left\{\frac{d}{dr^2}(r^2\Delta)\right\} - \frac{1}{4\bar{R}} + \frac{\bar{R}}{\bar{B}^2}\frac{dp}{dr^2} = 0 \ . \tag{53}$$

Integrating, and using the boundary conditions $\Delta(a^2) = 0$ (no shift of the boundary), and $\Delta(0)$ finite, we have

$$r^2\frac{\Delta}{\bar{R}} = \frac{r^4}{8\bar{R}^2} - \int_0^{r^2}\frac{p}{\bar{B}^2}\,dr^2 - \frac{a^2r^2}{8\bar{R}^2} + \frac{r^2}{a^2}\int_0^{a^2}\frac{p}{\bar{B}^2}\,dr^2 \tag{54}$$

For the particular initial equilibrium being considered we then have

$$\frac{\Delta}{\bar{R}} = -\frac{5}{8}x \tag{55}$$

Similarly for the initial state we have

$$\frac{\Delta_0}{\bar{R}} = -\frac{5}{8}(e - x) \tag{56}$$

From Ref. [6] we have

$$|\nabla r|^2 = 1 - 2\frac{d\Delta}{dr}\cos\theta + \frac{1}{2}\left(\frac{d\Delta}{dr}\right)^2 + \frac{3}{4}\frac{r^2}{\bar{R}^2} + \frac{\Delta}{\bar{R}} \tag{57}$$

which allows the following averaged quantities to be evaluated

$$\left\langle \frac{|\nabla r|^2 R_0^2}{R^2} \right\rangle = 1 + \frac{145}{32}e - \frac{123}{32}x \tag{58}$$

$$\langle |\nabla_0 r_0|^2 \rangle = 1 + \frac{69}{32}x - \frac{5}{8}e \,. \tag{59}$$

Similarly, we also have

$$\langle R_0^2/R^2 \rangle = 1 + 3e - 6x \tag{60}$$

We can now evaluate the initial and final energy functionals to give

$$\frac{W_i}{\pi^2\bar{R}^3\bar{B}^2} = e + (3\beta-1)e^2 + (3\beta - \frac{31}{32})e^3 + 0(e^4) \tag{61}$$

$$\frac{W_f}{\pi^2\bar{R}^3\bar{B}^2} = e + (3\beta-1)e^2 - (\beta - \frac{9}{32})e^3 + 0(e^4) \tag{62}$$

Since we must have $\beta > 1$ (for the initial pressure profile to be everywhere positive) we again see that the energy is lower after the interchange. The final pressure profile again takes the form shown in Fig.4.

V. Conclusions.

We have shown that a flat q-profile with q = 1, which permits the free interchange of flux tubes in ideal MHD, gives access to quasi-equilibrium states of lower energy. The transition to such a state can take place on a fast timescale, and corresponds in many respects to the sawtooth collapse seen in large tokamaks such as JET. In particular the final state has a hollow pressure profile.

The collapse of the central temperature during the sawtooth may occur through three routes: (a) quasi-interchange, as described in this paper, (b) a large amount of resistive reconnection, as in the original Kadomstev model [2] for instance, and (c) rapid diffusion along stochastic magnetic fields [7,8,9]. In practice a sawtooth collapse may involve a combination of more than one mechanism with one or another predominating, (depending possibly on the experimental circumstances), and this may provide a useful classification scheme. Note that conservation of helical flux [2] produces mixing of the high and low pressure regions for a strongly monotonic q-profile and so averages out the pressure profile. Also, diffusion along a stochastic field cannot give rise to a reversed radial pressure gradient. Thus processes (b) and (c) tend to flatten the pressure, and therefore hollow profiles arise only when process (a) predominates. Since quasi-interchange requires a flat q close to unity the observation of hollow final states on JET supports the idea of such a q-profile.

Recently direct measurements of q on-axis have been made on several experiments. On both TEXT [10] and TEXTOR [11] it is found that q(o) is significantly below unity during all phases of the sawtooth, with values typically around 0.7. By contrast, on ASDEX [12] q(o) is found to be close to unity. The resolution of this apparent conflict is unclear; however, one possibility is that there are different forms of sawteeth in which the value of q(o) determines which of the three processes discussed above is dominant.

The nature of the collapse mechanism leads to a relation between the radius of the $q = 1$ surface and the sawtooth inversion radius. A Kadomstev reconnection involving a strongly monotonic q-profile, for instance, predicts these to be about equal. For the cylindrical model with flat $q(r)$ discussed here, the strong toroidal field means the plasma is almost incompressible, and we have immediately

$$2\pi R \, \pi r(inv)^2 = 2\pi R \left\{\pi r(q = 1)^2 - \pi r(inv)^2\right\} \tag{63}$$

where $r(q=1)$ denotes the radius of the flat-q region, and thus

$$r(inv) = \frac{1}{\sqrt{2}} r(q = 1) \, . \tag{64}$$

The final state of the plasma in the non-linear model discussed in this paper is in MHD equilibrium but has a discontinuity in the pressure profile. In practice such a discontinuity will not arise as sharp gradients in pressure will be removed on a transport timescale by

diffusion and thermal conduction. This gives rise to the usual sawtooth heat pulse and density pulse. Departures from exact $q = 1$ require a small degree of resistive reconnection leading presumably to a hybrid timescale close to the ideal one. In such a case the gross predictions of the model should remain substantially unchanged.

Appendix A. Arbitrary Aspect Ratio Tokamak.

In this appendix we examine how in principle the final state may be calculated numerically at finite aspect ratio for any given initial equilibrium. This is best done through a variational formulation.

Consider first the case where the boundary of the $q = 1$ region is fixed. This is analagous to the cylindrical problem treated in section II. The initial magnetic field is given by

$$\underline{B}_0 = \frac{1}{R_0} \nabla_0 \psi_0 \times \underline{e}_\phi + \frac{1}{R_0} I_0(\psi_0) \underline{e}_\phi \tag{A1}$$

where ψ_0 satisfies the Grad-Shafranov equation

$$R_0^2 \nabla_0 \cdot (\frac{1}{R_0^2} \nabla_0 \psi_0) = -R_0^2 \frac{dp_0}{d\psi_0} - I_0 \frac{dI_0}{d\psi_0} \tag{A2}$$

and we assume that $p_0(\psi_0)$, $I_0(\psi_0)$ and $\psi_0(R, Z)$ are all known.

Consider an initial surface with poloidal flux ψ_0 which is mapped to a final surface with poloidal flux ψ. Since flux is preserved between any two flux surfaces we have $|\Delta\psi| = |\Delta\psi_0|$ (where $\Delta\psi_0$ is the flux between surfaces ψ_0 and $\psi_0 + \Delta\psi_0$, etc.), and so the mapping which inverts the order of the surfaces is given by

$$\psi(\underline{r}) = \psi_1 - \psi_0\ (\underline{r}_0) \qquad \text{(A3)}$$

where ψ_1 labels the (fixed) boundary of the $q = 1$ region.

From eq. (A2) the volume enclosed between the flux surfaces labelled by ψ and $\psi + \Delta\psi$ is given by

$$\Delta V(\psi) = 2\pi\ \Delta\psi \oint_{\psi} \frac{d\ell_p\ R}{|\nabla\psi|} \qquad \text{(A4)}$$

where $d\ell_p$ is the element of arc length along the line of constant ψ in the poloidal plane. Note that R and $|\nabla\psi|$ are to be expressed in terms of ψ and ℓ_p, and the integration is over the closed contour. Using conservation of entropy we then obtain the final pressure function in the form

$$p(\psi) = p_0(\psi_0) \left| \frac{dV_0}{dV} \right|^{\gamma}$$

$$= p_0(\psi_0) \left\{ \frac{\oint_{\psi_0} \frac{d\ell_p R_0}{|\nabla_0\psi_0|}}{\oint_{\psi} \frac{d\ell_p R}{|\nabla\psi|}} \right\}^{\gamma} \qquad \text{(A5)}$$

where ψ_o is found, for a given ψ, from eq. (A3). Note that the integration over the original surface ψ_0 can be performed since the original equilibrium is given, whereas the integration over the

corresponding final surface ψ cannot be done until the final equilibrium is known.

In a similar way the final state flux function is obtained from equation (A1) using conservation of flux to give

$$I(\psi) = I_0(\psi_0) \left\{ \frac{\oint_{\psi_0} \frac{d\ell_p}{|\nabla_0 \psi_0| R_0}}{\oint_{\psi} \frac{d\ell_p}{|\nabla\psi| R}} \right\} \tag{A6}$$

The remaining requirement is that the final state satisfy the Grad-Shafranov equation. We now show that this is equivalent to minimising the final state energy functional given by

$$W = \int dV \left\{ \frac{|\nabla\psi|^2}{2R^2} + \frac{I^2}{2R^2} + \frac{P}{\gamma - 1} \right\} \tag{A7}$$

subject to the entropy and flux constraints. This is essentially a special case of the variational principle of Kruskal and Kulsrud [13].

When $I(\psi)$ is varied at fixed position there is a term $I'(\psi)\delta\psi$ and a contribution δI due to the change in the functional form of $I(\psi)$. From eq. (A6) we have

$$\delta I = - I \, \delta\phi_\psi \frac{d\ell_p}{|\nabla\psi| R} \Big/ \oint_\psi \frac{d\ell_p}{|\nabla\psi| R} \tag{A8}$$

If we now use the relation

$$\oint_\psi \frac{d\ell_p}{|\nabla\psi| R} = \frac{1}{2\pi} \frac{d}{d\psi} \int_\psi \frac{dV}{R^2} \tag{A9}$$

where the volume integral is over the volume enclosed by the flux surface ψ, then we can write

$$\delta I = I \frac{d}{d\psi} \oint_\psi \frac{d\ell_p \, \delta\psi}{|\nabla\psi| R} \Big/ \oint \frac{d\ell_p}{|\nabla\psi| R} \tag{A10}$$

The variation in the energy due to the I^2 term is now easily evaluated using eq. (A10) and integrating by parts, making use of the identity

$$\int dV \, A = \int_0^{\psi_1} d\psi \oint_\psi \frac{d\ell_p}{|\nabla\psi|} 2\pi R \, A \tag{A11}$$

for any integrand A. The contributions from the pressure term and the poloidal field terms can be found in a similar way, giving a total energy variation

$$\delta W = - \int dV \; \delta\psi \left\{ \nabla \cdot \left(\frac{\nabla\psi}{R^2}\right) + \frac{I'I}{R^2} + p' \right\} . \qquad \text{(A12)}$$

Thus when the energy functional is stationary, the final state Grad-Shafranov equation is satisfied. The numerical solution can therefore be carried out by choosing trial functions for $\psi\,(R,Z)$ evaluating W from eq. (A7) using eq. (A5) and eq. (A6); the choice which minimises W giving the required approximate solution.

In principle this method can be extended to include displacements of the plasma outside the $q = 1$ region. Eq. (A3) then becomes

$$\begin{aligned} \psi\,(\underline{r}) &= \psi_1 - \psi_0\,(\underline{r}_0) \qquad 0 < \psi_0 < \psi_1 \\ \psi\,(\underline{r}) &= \psi_0(\underline{r}_0) \qquad\quad \psi_1 < \psi_0 < \psi_a \; . \end{aligned} \qquad \text{(A13)}$$

In deriving eq. (A12) we assumed continuity of p, I and $|\nabla\psi|$. For the two region problem this no longer holds and there is a contribution to δW from the ψ_1 surface given by

$$\delta W_s = - \left|\left| \oint_{\psi_1} d\ell_p \; R \, \frac{\delta\psi}{|\nabla\psi|} \; (p + \tfrac{1}{2} B^2) \right|\right| \qquad \text{(A14)}$$

where the double bars denote the jump across ψ_1. Since the displacement of the ψ_1 flux surface, given by $\xi_\psi = - \delta\psi \,/\, |\nabla\psi|$, must be continuous the final equilibrium must satisfy the force balance relation

$$\left|\left| \; (p + \frac{1}{2} B^2) \right|\right| = 0 \; . \qquad \text{(A15)}$$

We therefore minimise W using trial functions which satisfy eq. (A15).

Appendix B. Solution of the Cylindrical 2-Region Problem.

We examine here the extension of the cylindrical calculation of section II to include the effects of the plasma outside the $q = 1$ region.

Consider the q-profile defined by

$$q = 1 \qquad 0 \leq r_0 \leq a$$

$$q = \left\{1 - \frac{(r_0 - a)^2}{12a^2}\right\}^{-1/2} \qquad a \leq r_0 \leq A \qquad \text{(B1)}$$

which is plotted in Fig. 2. The fixed boundary of the plasma is at $r_0 = A$, and we take $A = 2a$. We look for an initial-state equilibrium having this q-profile and (as in section II) a uniform toroidal field $B_z^2 = b_0^2 = \text{constant}$. We require the pressure to vanish at the boundary,

$$p_0(r_0 = A) = 0$$

and we also demand force balance across the surface $r_0 = a$ (see Appendix A):

$$\left|\left| p_0 + \frac{B_0^2}{2} \right|\right| = 0 \ . \qquad \text{(B2)}$$

Solution of the equilibrium equation then gives the following pressure profile:

$$p_0(x) = \frac{b_0^2}{2}\left\{\frac{17}{4}e - 2x\right\}$$

$$0 \leq x \leq e \qquad \text{(B3)}$$

$$p_0(x) = \frac{b_0^2}{2}\left\{\frac{17}{4}e - 2x + -\frac{(x-e)^2}{12e}\ \frac{(x-e)^3}{9e^2}\right\}$$

$$0 \leq x \leq 4e \qquad \text{(B4)}$$

where, as before, $x = r_o^2/\bar{R}^2$, $e = a^2/\bar{R}^2$ and $\bar{R}$ is a constant.

We now seek a mapping of initial flux surfaces into final flux surfaces, which preserves the order of the surfaces for $x > e$, but which reverses the order of the surfaces for $x < e$. Suppose the surface at $x = e$ is mapped to $x_f = \lambda e$. Then we can write the mapping in the form

$$h_1(x) = 1 + \frac{F_1^2(x)}{\bar{R}^2}$$

$$= 1 + \lambda(e - x) + Y_1(x)$$

$$0 \leq x \leq e \qquad \text{(B5)}$$

$$h_2(x) = 1 + \frac{F_2^{\,2}(x)}{\bar{R}^2}$$

$$= 1 + \frac{x}{3}(4 - \lambda) + \frac{4}{3} e (\lambda - 1) + Y_2(x)$$

$$e \leq x \leq 4e \qquad \text{(B6)}$$

where $Y_1(0) = Y_1(e) = Y_2(e) = Y_2(4e) = 0$. Such a mapping is illustrated in Fig.5. Because of the strong toroidal field, $Y_1 \sim Y_2 \sim 0(e^2)$ and $\lambda = 1 + \delta$ where $\delta \sim 0(e^2)$. From the final state equilibrium equation (eq.(10)) for the region $x < e$, and using the mapping $h_1(x)$, we obtain

$$Y_1(x) = - x(e - x) \qquad \text{(B7)}$$

to leading order. Similarly for the region $x > e$ with the mapping $h_2(x)$ the final state equilibrium equation gives $Y_2(x) = 0$, to the same order. Force balance in the final state across the surface $x = \lambda e$ requires

$$\left|\left| p + \frac{B^2}{2} \right|\right| = 0 \qquad \text{(B8)}$$

which gives

$$\delta = \frac{3}{2} e \qquad \text{(B9)}$$

We now have an explicit mapping from initial to final states, which

together with the initial equilibrium allows initial and final state energies to be calculated. We obtain

$$\frac{W_i}{\pi^2 \bar{R}^3 b_0^2} = 4e + \frac{185}{16} e^2 \tag{B10}$$

$$\frac{W_f}{\pi^2 \bar{R}^3 b_0^2} = 4e + \frac{185}{16} e^2 - \frac{997}{96} e^3 \tag{B11}$$

so again the final state has lower energy. Note the $(W_f - W_i)/W_i$ is larger here than was found in Section II; the freedom to expand the plasma in the inner region has allowed a lower final state energy.

References

[1] D.J. Campbell et. al., Nucl. Fusion Letters 26, 1085 (1986)

[2] B.B. Kadomstev, Sov. J. Plasma Physics, 1, 389 (1975)

[3] J.A. Wesson, JET Report JET-P(85)25, JET Joint Undertaking, Abingdon, Oxfordshire, U.K. (1985)

[4] A.W. Edwards et. al., Phys. Rev. Lett. 57, 210 (1986)

[5] J.A. Wesson et. al., Proc. 11th International Conference on Plasma Physics and Controlled Fusion, IAEA, Kyoto, vol.2, 3 (1986)

[6] J.W. Connor and R.J. Hastie, Culham Laboratory Report CLM-M106, UKAEA Culham Laboratory, Abingdon OX14 3DB, UK (1985)

[7] M. Dubois and A. Samain, Nucl. Fusion 20, 1101 (1980)

[8] C. Mercier, Sov. J. Plasma Physics 9, 82 (1983)

[9] A.J. Lichtenberg, Nucl. Fusion 24, 1277 (1984)

[10] W.P. Wert. et. al., Phys. Rev. Lett. 58, 2758, (1987)

[11] H.Soltwisch et. al., Proc. 11th International Conference on Plasma Physics and Controlled Fusion, IAEA, Kyoto, Vol.I, 263 (1986).

[12] K. McCormick et. al., Proc. 12th European Conf. Budapest, vol. I, 199 (1985)

[13] M.D. Kruskal and R. M. Kulsrud, Phys. Fluids 1, 265 (1958)

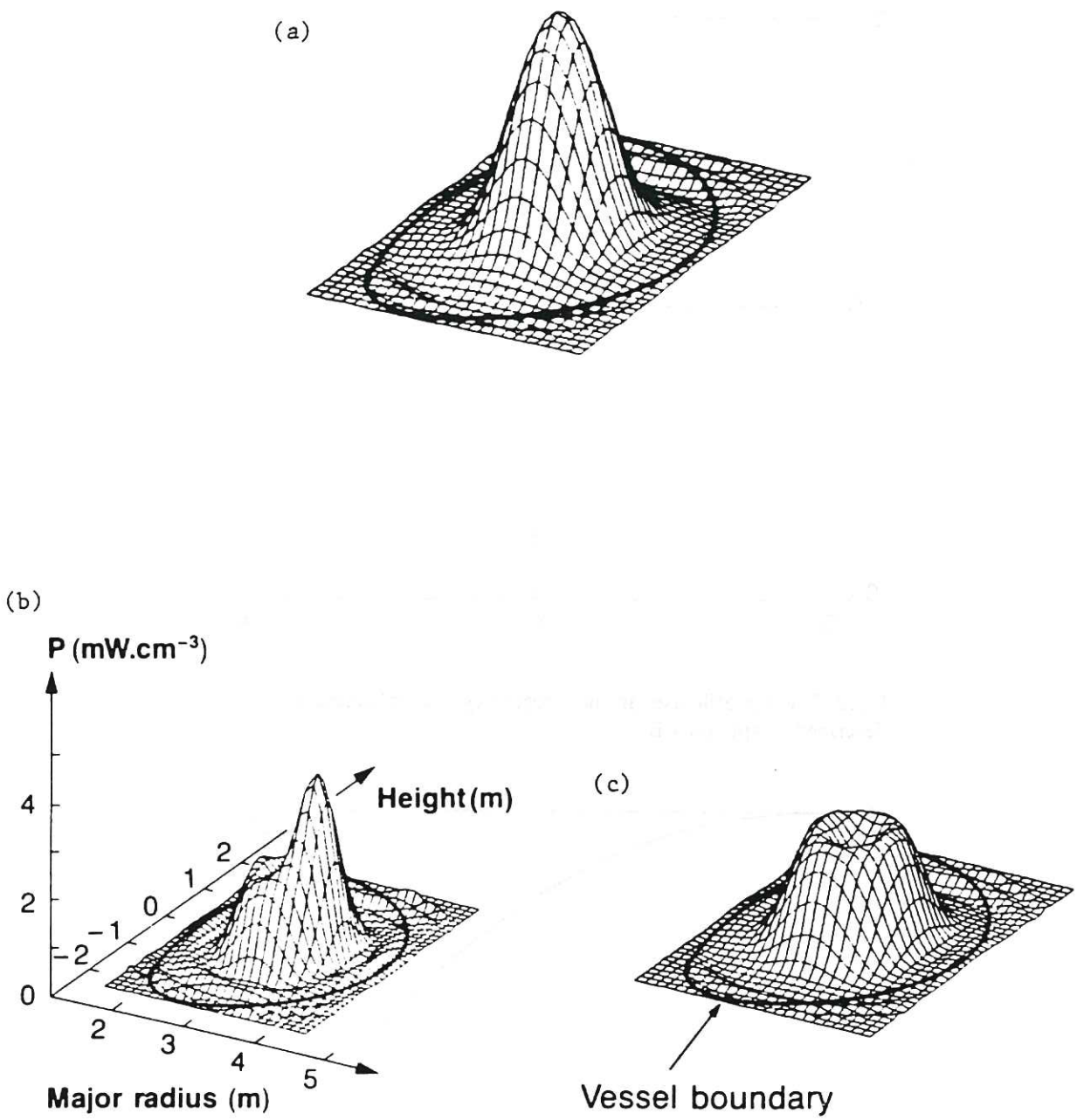

Fig. 1 Results from soft X-ray tomography on JET showing (a) the profile before the start of the collapse ($t'=0$), (b) an early stage of the collapse ($t'=300\,\mu$s), and (c) the final state with a hollow profile ($t'=2980\,\mu$s). (Reproduced from Ref. [4] with the kind permission of JET Joint Undertaking).

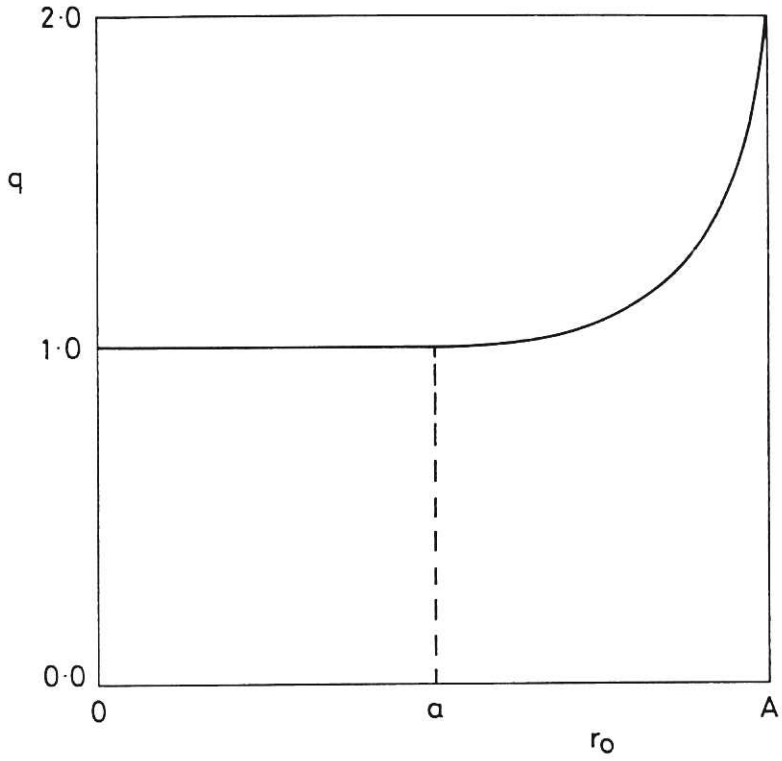

Fig. 2 The q-profile used in the 2-region cylindrical calculation described in appendix B.

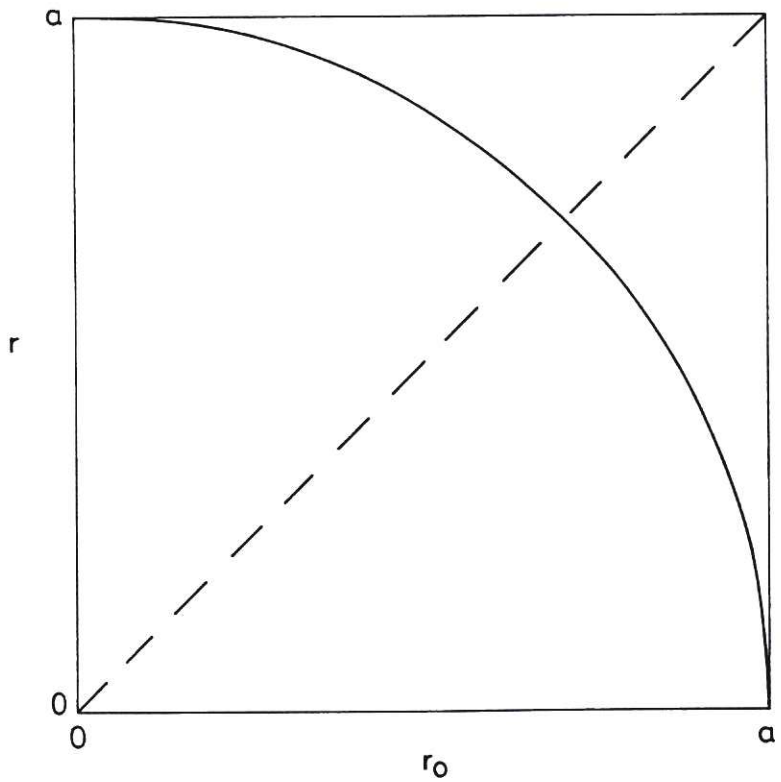

Fig. 3 The mapping of initial flux surfaces into final flux surfaces. The dashed line shows the identity map.

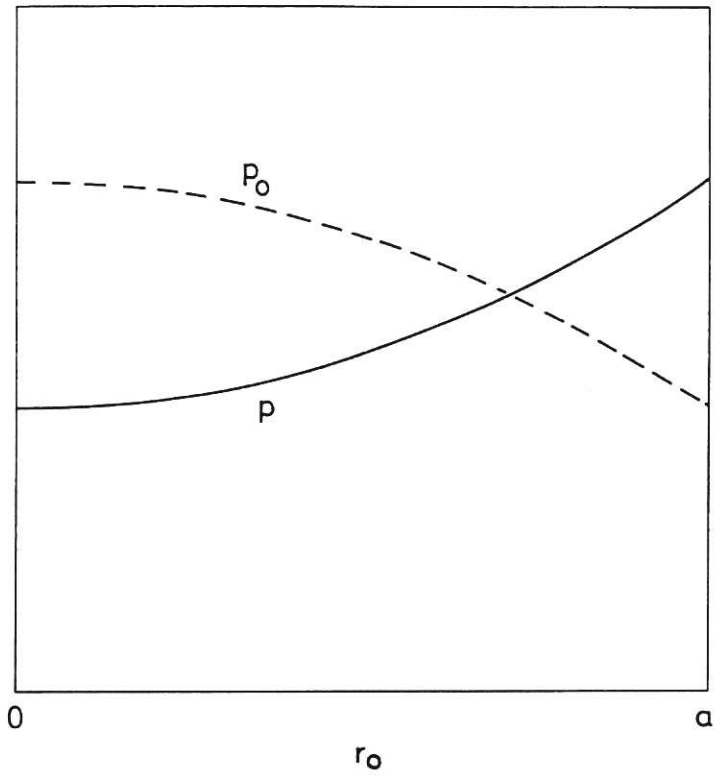

Fig. 4 The initial and final pressure profiles.

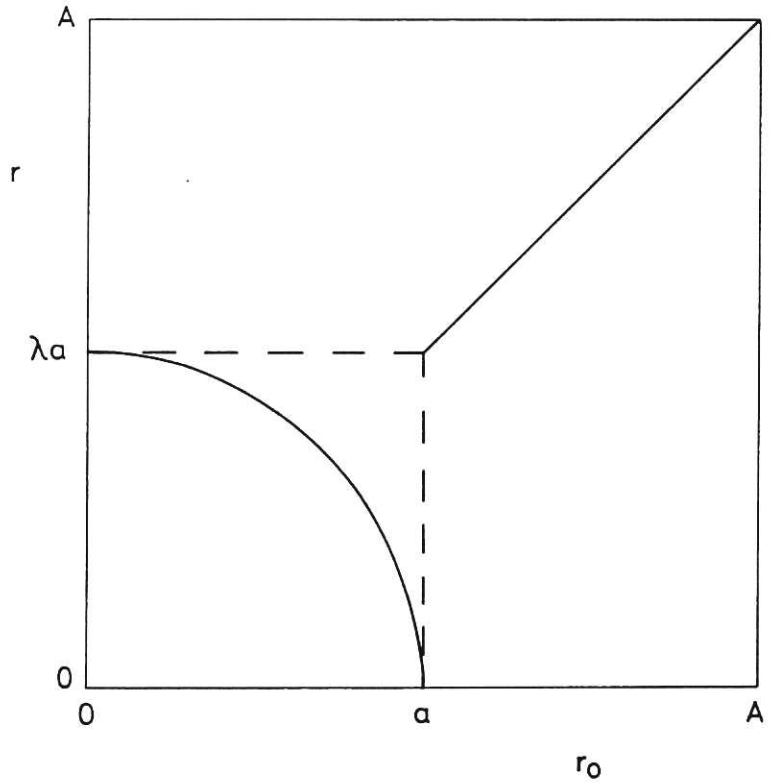

Fig. 5 The mapping function for the 2-region problem.